Electronic Supporting Information to accompany:

Investigating the Role of Amine in InP Nanocrystal Syntheses: Destabilizing Cluster Intermediates by Z-Type Ligand Displacement

Dylan C. Gary, Alessio Petrone, Xiaosong Li, and Brandi M. Cossairt*

Experimental Details

Indium acetate (99.99%), α, α, α trifluorotoluene (>99%), and phenylacetic acid (99%) were purchased from Sigma-Aldrich and used without further purification. Toluene, ethyl acetate, and pentane were purchased from various sources. NMR solvents were purchased from Cambridge Isotope Laboratories. All solvents were dried over calcium hydride, distilled, and stored over 4 Å molecular sieves prior to use. Benzylamine (99%) and 4-fluorobenzylamine (97%) were purchased from Sigma Aldrich and dried over calcium hydride, distilled, and stored over 4 Å molecular sieves prior to use. $P(Si(CH_3)_3)_3$ was prepared according to literature procedures.[1] All manipulations were performed under an inert atmosphere of dry N_2 using standard Schlenk or glovebox techniques unless otherwise stated. Optical spectra were acquired on a Cary 5000 UV-Vis-NIR spectrophotometer from Agilent Technologies. NMR spectra were acquired on 500 MHz Bruker Avance spectrometers.

Synthesis of $In_{37}P_{20}(O_2CCH_2C_6H_5)_{51}$: $In_{37}P_{20}(O_2CCH_2C_6H_5)_{51}$ was prepared by modification of a reported procedure for myristate-capped particles using $In(O_2CCH_3)_3$ (934 mg, 3.20 mmol) and phenylacetic acid (1.58 g, 11.6 mmol) in toluene (10 mL), and $P(Si(CH_3)_3)_3$ (465 μL, 1.60 mmol) in toluene (5 mL).[2] The workup procedure was modified from that of the particles with a myristate ligand set by substituting pentane for acetonitrile to selectively precipitate the particles (three cycles). $In_{37}P_{20}(O_2CCH_2C_6H_5)_{51}$ was isolated in 25% yield (238 mg, 0.02 mmol) based on $P(Si(CH_3)_3)_3$ as the limiting reagent.

Crystallization Procedure for $In(O_2CCH_2C_6H_5)_3(H_2NCH_2C_6H_5)_3$: Under a nitrogen atmosphere $In_{37}P_{20}(O_2CCH_2C_6H_5)_{51}$ (100 mg) was dissolved in ethyl acetate (1 mL). Using a microliter glass syringe, 100 μL of benzylamine was added to the vial and the solution was filtered into a scintillation vial using a 1 mL syringe outfitted with a PFTE filter with a 0.45 μm pore size. Small, white needles were found in the scintillation vial after about one week at room temperature.

Crystallization Procedure for $In(O_2CCH_2C_6H_4F)_4(H_3NCH_2C_6H_5)$: In a nitrogen filled glovebox, $In_{37}P_{20}(O_2CCH_2C_6H_5)_{51}$ (117mg) was weighed directly into a J Young NMR tube. CD_2Cl_2 (0.5 mL) was then added to the J. Young tube. $H_2NCH_2C_6H_5$ was added (3 μL) and a yellow precipitate was observed in the NMR tube the next day. The precipitate was redissolved by adding ~2 mL of toluene to the J Young tube, sealing the tube, bringing the tube out of the glovebox, and then sonicating the tube for an hour at 60 °C. The tube was then allowed to slowly come to room temperature. Small, yellow needles formed after approximately 12 hours at room temperature.

Single Crystal X-Ray Diffraction Methods for $In(O_2CCH_2C_6H_5)_3(H_2NCH_2C_6H_5)_3$: A colorless needle, measuring 0.19 x 0.03 x 0.03 mm3 was mounted on a loop with oil. Data was collected at -173 °C on a Bruker APEX II single crystal X-ray diffractometer, Mo-radiation.

Titration of $In_{37}P_{20}(O_2CCH_2C_6H_5)_{51}$ with $H_2NCH_2C_6H_4F$ for ^{19}F, ^{31}P, and ^1H NMR spectroscopy: $In_{37}P_{20}(O_2CCH_2C_6H_5)_{51}$ (107 mg) was weighed directly into a J Young tube in a nitrogen filled glovebox using weight paper as a funnel. CD_2Cl_2 (0.5 mL) was added to the J Young tube. α, α, α trifluorotoluene

(17 μL) was added to the tube as an internal standard for ^{19}F NMR. For each addition of $H_2NCH_2C_6H_4F$, 1μL of $H_2NCH_2C_6H_4F$ was added with a microliter syringe. ^{31}P, ^{19}F, and ^{1}H NMR spectra were acquired between each addition of $H_2NCH_2C_6H_4F$.

Titration of $In_{37}P_{20}(O_2CCH_2C_6H_5)_{51}$ with $H_2NCH_2C_6H_4F$ for UV-Vis: $In_{37}P_{20}(O_2CCH_2C_6H_5)_{51}$ (31 mg) was weighed out into a 100 mL volumetric flask in a nitrogen filled glovebox and toluene was added to the flask to dissolve $In_{37}P_{20}(O_2CCH_2C_6H_5)_{51}$ and dilute to the mark. A microliter syringe was used to add 26.6 μL of $H_2NCH_2C_6H_4F$ to a 5 mL volumetric flask. Toluene was added to the 5 mL flask and filled to the mark. For each spectrum, a 500 μL syringe was used to measure out 1 mL of $In_{37}P_{20}(O_2CCH_2C_6H_5)_{51}$ stock solution into a cuvette to which 10 μL of the $H_2NCH_2C_6H_4F$ stock solution was added for every equivalent of $H_2NCH_2C_6H_4F$ intended for the final solution. The cuvette was sealed with a screw cap and electrical tape and brought out of the glovebox and the spectrum was acquired.

Computational Methods. Computational studies were performed using the *Gaussian* electronic structure package.[3] The HSE06[4-7] range-separated hybrid DFT functional was used to perform both the linear-response TDDFT absorption spectra and geometry optimizations. This method is appropriate for describing charge-transfer excitations and has been previously shown to correctly compute the InP quantum dot electronic structure.[8, 9] TDDFT[10-12] was used to compute both the excitation energies and corresponding oscillator strengths of the first 10 electronic transitions. The LANL2DZ basis set is used, in which core electrons are replaced by an effective core potential, and only O (1s, 2s, 2p), C (1s, 2s, 2p), In (5s, 5p) and P (3s, 3p) atomic orbitals are described with explicit basis functions.[13-16]

In order to investigate the effect of an under-coordinated phosphorus atoms on the UV-Vis spectrum, a structure was used where the In16 and the three closest carboxylate ligands were removed from the air-free $In_{37}P_{20}(O_2CCH_2C_6H_5)_{51}$ structure previously studied.[9]

To further investigate the effect of the structural rearrangement on the electronic properties, geometry optimizations on structures where the phenyl moieties were replaced by acetate, $In_{37}P_{20}(O_2CCH_3)_{51}$ and $In_{36}P_{20}(O_2CCH_3)_{48}$, were also performed.

Supplementary Figures and Analysis

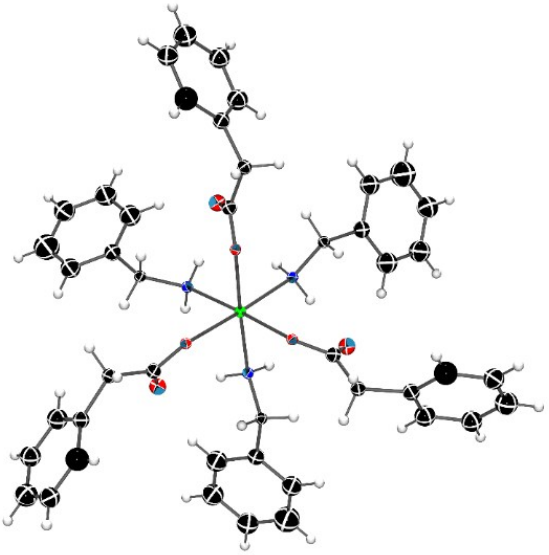

Figure S1. Crystal structure of $In(O_2CCH_2C_6H_5)_3(H_2NCH_2C_6H_5)_3$ with thermal ellipsoids at the 50% probability level obtained by addition of 108 equivalents of $H_2NCH_2C_6H_5$ to $In_{37}P_{20}(O_2CCH_2C_6H_5)_{51}$. The unit cell contains three $In(O_2CCH_2C_6H_5)_3(H_2NCH_2C_6H_5)_3$ molecules. Only one $In(O_2CCH_2C_6H_5)_3(H_2NCH_2C_6H_5)_3$ molecule is depicted here for clarity. Crystallographic data may be retrieved from the Cambridge Crystallographic Database under deposition number 1507652.

Assignment of Solution Phase $^{31}P\{^1H\}$ NMR Spectrum of $In_{37}P_{20}(O_2CR)_{51}$: UV-Vis absorbance spectroscopy and PDF analysis (Figure S2 and S3) suggest that the inorganic core from the crystal structure of $In_{37}P_{20}(O_2CCH_2C_6H_5)_{51}$ should be general for alkyl carboxylate ligated InP MSCs.

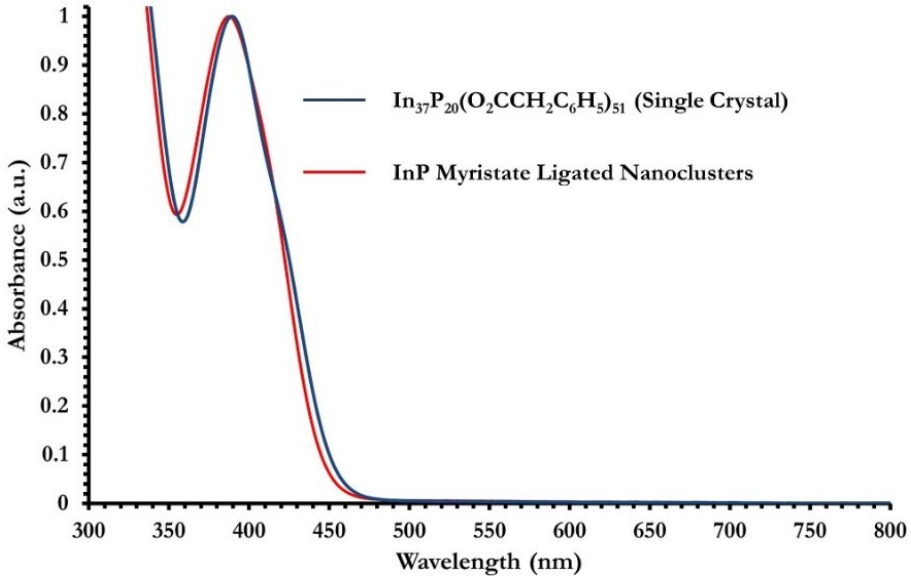

Figure S2. Normalized UV-Vis absorbance spectra of single crystals of $In_{37}P_{20}(O_2CCH_2C_6H_5)_{51}$ and a solution of InP myristate ligated nanoclusters. Both spectra match well with the spectrum predicted from the crystal structure of $In_{37}P_{20}(O_2CCH_2C_6H_5)_{51}$ by TDDFT.[9]

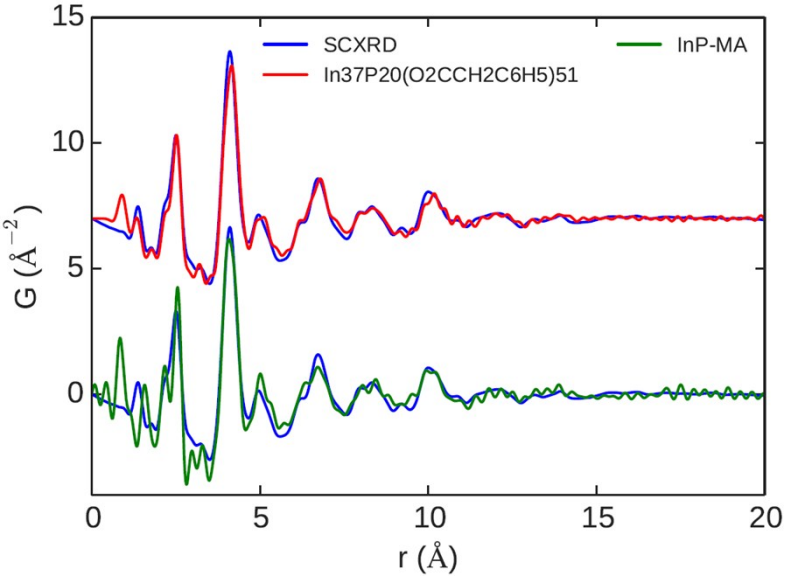

Figure S3. Comparison of PDF Analysis of $In_{37}P_{20}(O_2CCH_2C_6H_5)_{51}$, InP myristate capped clusters. The spectra and fits to the predicted pattern for the single crystal are in good agreement and suggest that the identity of the myristate ligated clusters are $In_{37}P_{20}(O_2C(CH_2)_{12}CH_3)_{51}$.

With this information and the crystal structure of $In_{37}P_{20}(O_2CCH_2C_6H_5)_{51}$, it should be feasible to give a tentative assignment to the $^{31}P\{^1H\}$ NMR of carboxylate ligated InP MSCs. The $^{31}P\{^1H\}$ NMR spectrum

of the oleate ligated clusters is the most straightforward to assign given that it has sharper peaks with better separation than the $^{31}P\{^{1}H\}$ NMR spectrum of $In_{37}P_{20}(O_2CCH_2C_6H_5)_{51}$. In order to determine the minimal delay time needed between pulses such that each ^{31}P environment would be integrated quantitatively, an inversion recovery experiment was performed to determine T1 times for ^{31}P in InP oleate clusters. This experiment suggested that the minimal delay time between pulses should be about 40 seconds for integration of the ^{31}P resonances to be 99% accurate.[17] If the integral of the peak furthest downfield in the $^{31}P\{^{1}H\}$ NMR spectrum of $In_{37}P_{20}(O_2C(CH_2)_7CH{=}CH(CH_2)_7CH_3)_{51}$ is normalized to 1, then each other integration is within 0.1 of the integers of 1, 2, or 4 and sum to 20, with two peaks integrating for one, which is consistent with the structural model of the $In_{37}P_{20}$ core in $In_{37}P_{20}(O_2CCH_2C_6H_5)_{51}$ wherein two chemically unique P atoms lay on the C_2 axis of the molecule (Figure S4).

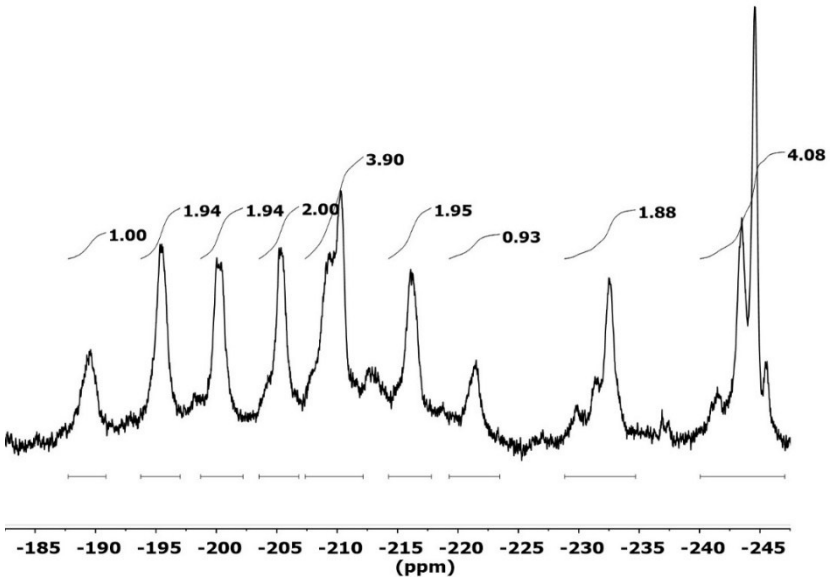

Figure S4. $^{31}P\{^{1}H\}$ NMR spectrum of $In_{37}P_{20}(O_2C(CH_2)_7CH{=}CH(CH2)_7CH_3)_{51}$ taken at 202.3 MHz in C_6D_6.

We begin the assignment of the ^{31}P NMR spectrum of $In_{37}P_{20}(O_2C(CH_2)_7CH{=}CH(CH2)_7CH_3)_{51}$ with the two ^{31}P nuceli that are unique in the crystal structure of $In_{37}P_{20}(O_2CCH_2C_6H_5)_{51}$, namely those that are bisected by the C2 axis for the C2 symmetry of the core. These two ^{31}P environments are therefore the resonances at –189.5 and –221.5 ppm as these are the only two peaks that integrate to 1. These two peaks are separated in chemical shift by a difference of 32 ppm. Given that all P atoms in the cluster are in a pseudo tetrahedral environment with four In–P bonds, in order to account for this difference in chemical shift we need to determine a relative measure of the shielding felt by each phosphorus atom in the cluster. In order to account for shielding, an analysis was performed where the bonding environment was analyzed by classifying each indium atom according to the number of In–O bonds it possessed (Tables S1 - S3). Indium atoms that have more In–O bonds are considered more electron withdrawing since oxygen is more electronegative than phosphorus and therefore a phosphorus atom bound to indium atoms with more In–O bonds will be expected to come in further downfield.

	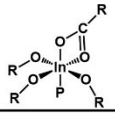	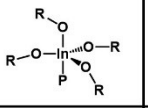	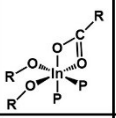	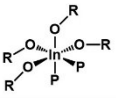	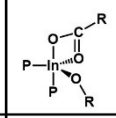	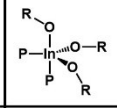		
In-P Bond Count	1	1	2	2	2	2	3	4
In-O Bond Count	5	4	4	4	3	3	1	0
# of In Atoms in Cluster	8	2	2	6	2	2	8	7

Table S1. Description of the 1st coordination sphere for every indium atom in $In_{37}P_{20}(O_2CR)_{51}$.

By applying this counting method to the two unique ^{31}P environments observed in $In_{37}P_{20}(O_2CR)_{51}$, the phosphorus atom that is bound to two surface indium atoms (shown as the P10 in Figure S5) is predicted to be the most deshielded, and therefore the most downfield. This is consistent with the observation that one of the two peaks in the $^{31}P\{^1H\}$ NMR spectrum of $In_{37}P_{20}(O_2C(CH_2)_7CH{=}CH(CH_2)_7CH_3)_{51}$ that integrates to 1 is the peak that comes in most downfield. In contrast, the most shielded ^{31}P environments should be those closest to the core. There are only two phosphorus atoms (P8 and P17) that are bound to indium centers that only exhibit In–P bonds. These two phosphorus atoms should appear most upfield, but the most upfield peak was previously assigned as a multiplet that integrated to about 4. If we treat this multiplet as two doublets we obtain integrations of about 1.9 and 2.2 which would now be consistent with assignment. The next furthest upfield resonances would be the other pair of phosphorus atoms bound to the central indium atom which is located in the center of the cluster (P7 and P1). The next furthest upfield resonance is predicted to be for the pair of phosphorus atoms (P11 and P2) that are located the shortest distance away from the single phosphorus atom predicted to be most downfield (P4). All other phosphorus nuclei in $In_{37}P_{20}(O_2CR)_{51}$ should experience approximately the same shielding according to this method and are indeed adjacent to each other by our assignment so far (Tables S1 - S3, and Figure S6).

Phosphorus Atom	Indium Atoms Bound to Phosphorus Atoms	Oxygen Atoms Bound to Those Indium Atoms
P(8) and P(17) (most upfield)	In(6) In(1) In(5) In(7) In(6) In(18) In(13) In(15)	None
P(7) and P(1) (2nd most upfield)	In(2) In(8) In(3) In(6) In(18) In(13) In(15)	O(71) O(70) O(53) O(13) O(38) O(59)
P(11) and P(2) (doublet 3rd most upfield)	In(21) In(3) In(18) In(12) In(25) In(14) In(1) In(2)	O(71) O(59) O(99) O(83) O(74) O(58) O(53) O(38) O(20) O(34) O(11) O(26)
P(4) (singlet 4th most upfield)	In(7) In(15) In(29) In(20)	O(66) O(31) O(75) O(48) O(29) O(22)
P(16) and P(12)	In(31) In(15) In(8) In(5) In(17) In(7) In(13) In(11)	O(13) O(21) O(16) O(24) O(18) O(70) O(76) O(68) O(40) O(62)
P(13) and P(19) (unassigned)	In(22) In(10) In(1) In(9) In(34) In(18) In(28) In(30)	O(12) O(1) O(10) (O2) O(63) O(51) O(9) O(96) O(19) O(46) O(73) O(78) O(89) O(77) O(85) O(90) O(87) O(84)
P(9) and P(14) (unassigned)	In(19) In(5) In(2) In(10) In(32) In(13) In(12) In(28)	O(38) O(12) O(1) O(10) O(2) O(17) O(3) O(5) O(6) O(14) O(71) O(73) O(78) O(89) O(61) O(92) O(81) O(82) O(69)
P(5) and P(20)	In(9) In(24) In(7) In(4) In(35) In(30) In(15) In(37)	O(63) O(65) O(50) O(39) O(47) O(101) O(95) O(102) O(67) O(93) O(88) O(15) O(94) O(46) O(30) O(23) O(28) O(27)
P(15) and P(6)	In(30) In(36) In(13) In(29) In(9) In(26) In(5) In(20)	O(46) O(66) O(31) O(75) O(91) O(79) O(77) O(45) O(80) O(48) O(29) O(22) O(63) O(4) O(2) O(7) O(8) O(64)
P(18) and P(3) (unassigned)	In(33) In(8) In(18) In(37) In(23) In(1) In(11) In(4)	O(70) O(25) O(41) O(42) O(54) O(52) O(101) O(95) O(102) O(67) O(93) O(88) O(15) O(94) O(13) O(57) O(55) O(56) O(86) O(60)
P(10) (least upfield)	In(16) In(27) In(14) In(3)	O(53) O(59) O(33) O(36) O(37) O(97) O(35) O(100) O(72) O(43) O(98) O(44)

Table S2. Inventory of every ^{31}P environment (1st column), each indium atom bound to those ^{31}P nuclei (2nd column), and every oxygen atom bound to those indium atoms (3rd column). ^{31}P nuclei that have been definitively assigned are colored according to their assignment in Figure S4 and S5. Atom numbers come from the cif file accompanying the crystal structure of $In_{37}P_{20}(O_2CCH_2C_6H_5)_{51}$.

Phosphorus Atom	Total Number of In-O Bonds	In-O Bonds per P atom	Chemical Shift (ppm)
P(8) and P(17) (most upfield)	0	0	-244.5
P(7) and P(1) (2nd most upfield)	6	3	-243.5
P(11) and P(2) (3rd most upfield)	12	6	-232.5
P(4) (4th most upfield)	12	6	-221.5
P(16) and P(12)	10	5	-216.1
P(13) and P(19)	18	9	Unassigned
P(9) and P(14)	18	9	Unassigned
P(5) and P(20)	18	9	Unassigned
P(15) and P(6)	18	9	Unassigned
P(18) and P(3)	20	10	-195.5
P(10) (most downfield)	12	12	-189.6

Table S3. Inventory of every ^{31}P environment (1st column) the total number of In–O bonds for every indium atom that ^{31}P environment is bound to (2nd column), and the total number of oxygen atoms bound to those indium atoms (3rd column). ^{31}P that have been definitively assigned are colored according to their assignment in Figure S4 and S5. Based upon the total number of In–O bonds, P(18) and P(3) are likely to lie just upfield of P(10), and P(16) and P(12) are likely to be the peak just downfield of P(4) (Figure S5).

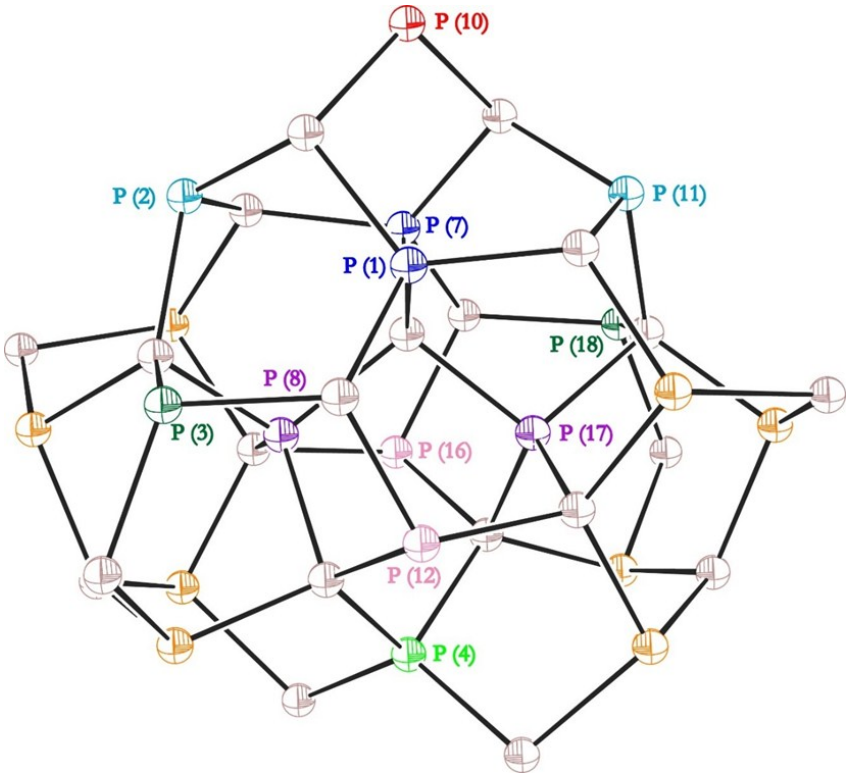

Figure S5. Diagram of every phosphorus atom in the core $[In_{21}P_{20}]^{3+}$. Each phosphorus atom and its label (except for those that cannot be unambiguously assigned in the ^{31}P NMR spectrum) are colored to match Figure S6.

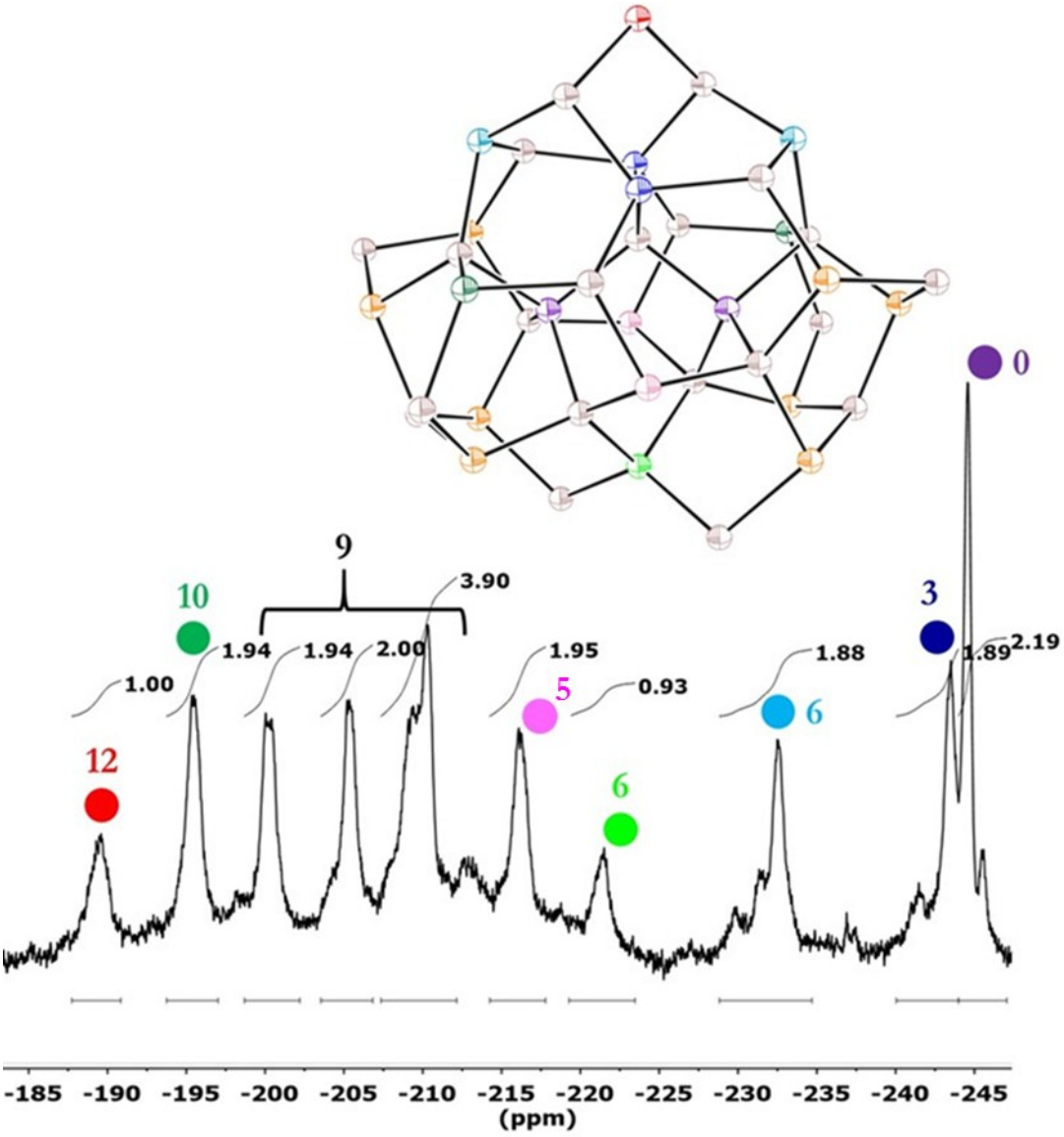

Figure S6. Assignment of $^{31}P\{^{1}H\}$ NMR spectrum of $In_{37}P_{20}(O_2C(CH_2)_7CH{=}CH(CH_2)_7CH_3)_{51}$ based upon the crystal structure of $In_{37}P_{20}(O_2CCH_2C_6H_5)_{51}$, the C2 symmetry of the core of the cluster, and the first coordination sphere of each indium metal center. The colored numbers indicate the sum of all In–O bonds for each of the 4 indium atoms bound to that ^{31}P environment. The sum of all In–O bonds from each of the 4 indium atoms bound to each unassigned ^{31}P environment is 9. Gray ellipsoids are indium and orange ellipsoids are unassigned phosphorus atoms.

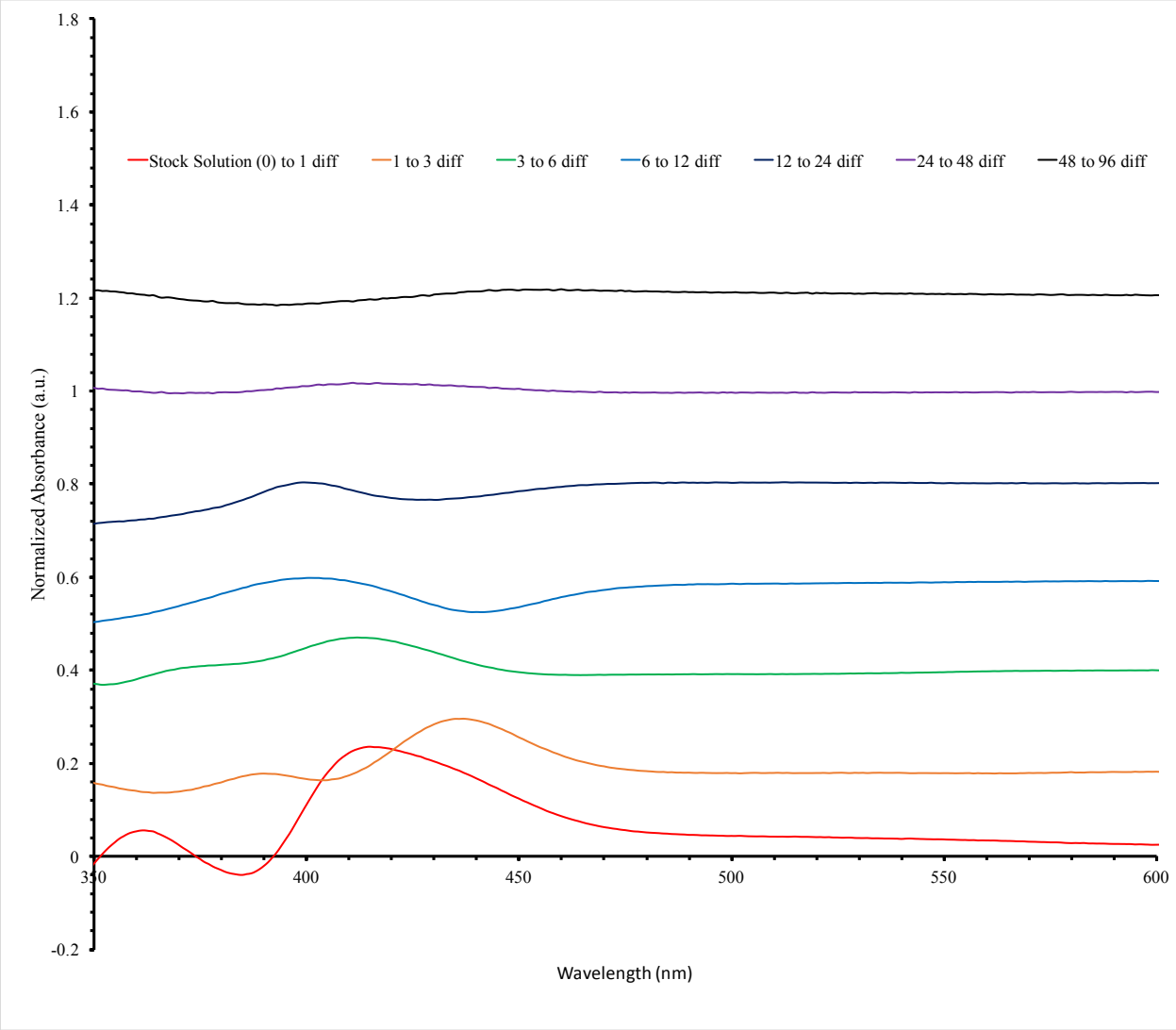

Figure S7. Difference spectra for sequential pairs of absorption spectra (raw data) on titration of $In_{37}P_{20}(O_2CCH_2C_6H_5)_{51}$ with $H_2NCH_2C_6H_4F$ showing the major changes in electronic structure on addition of the first 12 equivalents of amine and stabilization of the structure thereafter.

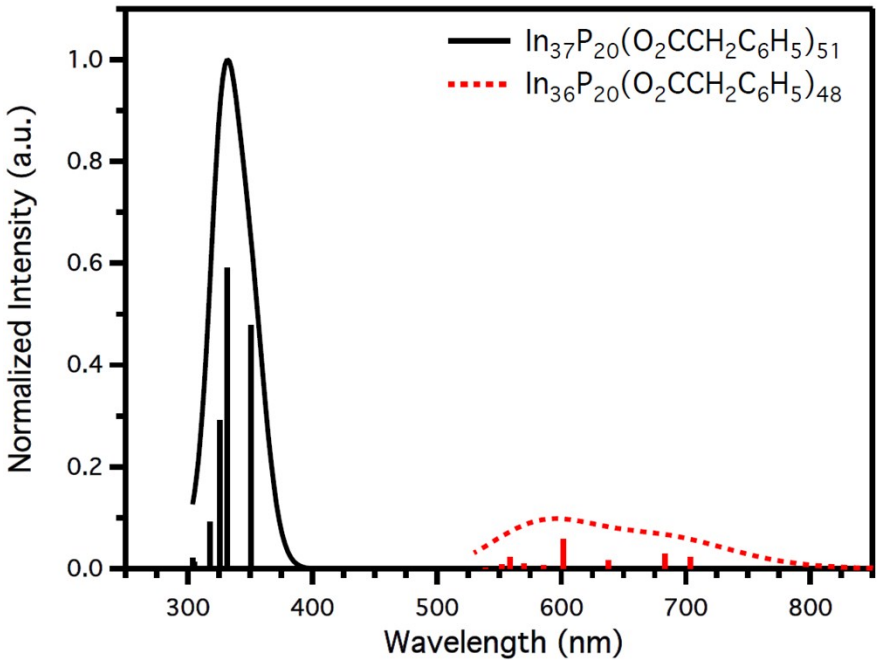

Figure S8. TD-HSE06/LANL2DZ optical spectra obtained from the first 10 individual optical transitions for the $In_{37}P_{20}(O_2CCH_2Ph)_{51}$ (black) crystallographic structure and the one where In16 and the three closest carboxylate ligands were removed, $In_{36}P_{20}(O_2CCH_2C_6H_5)_{48}$ (red). A Gaussian smoothing function (width 0.12 eV) has been used and all intensities are normalized respect to the highest peak.
Only the transitions relative to the first peaks have been shown for clarity.

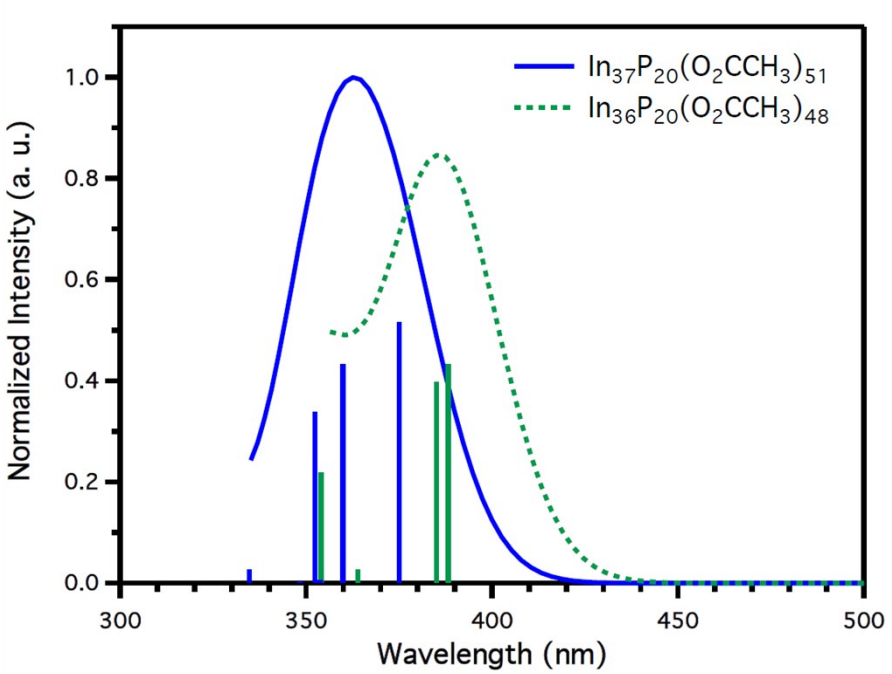

Figure S9. TD-HSE06/LANL2DZ optical spectra obtained from the first 10 individual optical transitions for the optimized acetate analog structures $In_{37}P_{20}(O_2CCH_3)_{51}$ (blue) and the one where In16 and the three closest carboxylate ligands were removed, $In_{36}P_{20}(O_2CCH_3)_{48}$ (green). The data for $In_{36}P_{20}(O_2CCH_3)_{48}$ is for the geometry optimized structure. A Gaussian smoothing function (width 0.12 eV) has been used and all intensities are normalized respect to the highest peak. Only the transitions relative to the first peak have been shown for clarity.

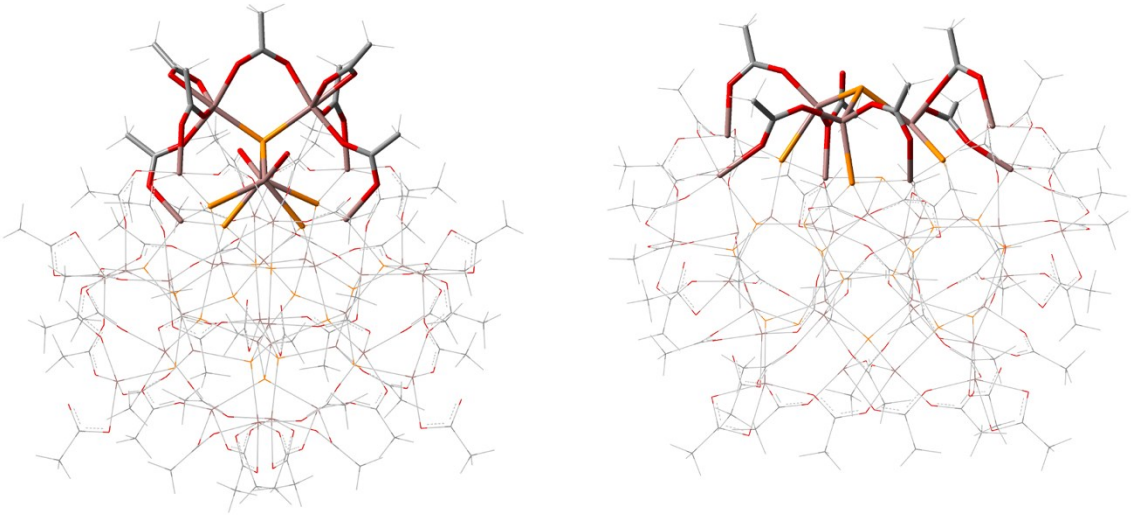

Figure S10. Molecular representation of the HSE06/LANL2DZ optimized structures of $In_{37}P_{20}(O_2CCH_3)_{51}$ (left) and $In_{36}P_{20}(O_2CCH_3)_{48}$ (right). Phosphorus is in yellow, indium in pink, carbon in dark gray, oxygen in red, and hydrogen in light gray. Only the atoms mostly affected by the reorganization have been highlighted in the figure, while the remaining ones are represented as a wireframe.

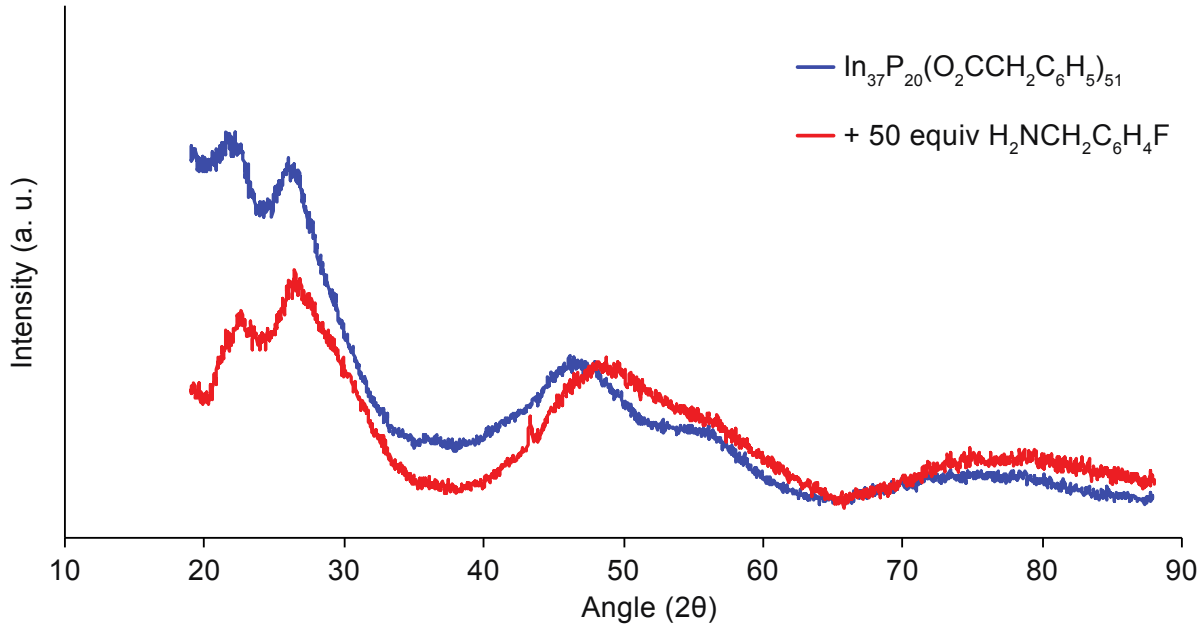

Figure S11. Powder X-ray diffraction data of $In_{37}P_{20}(O_2CCH_2C_6H_5)_{51}$ (blue) and amine-treated clusters (red) showing a broadening and shift to larger angles upon treatment with amine.

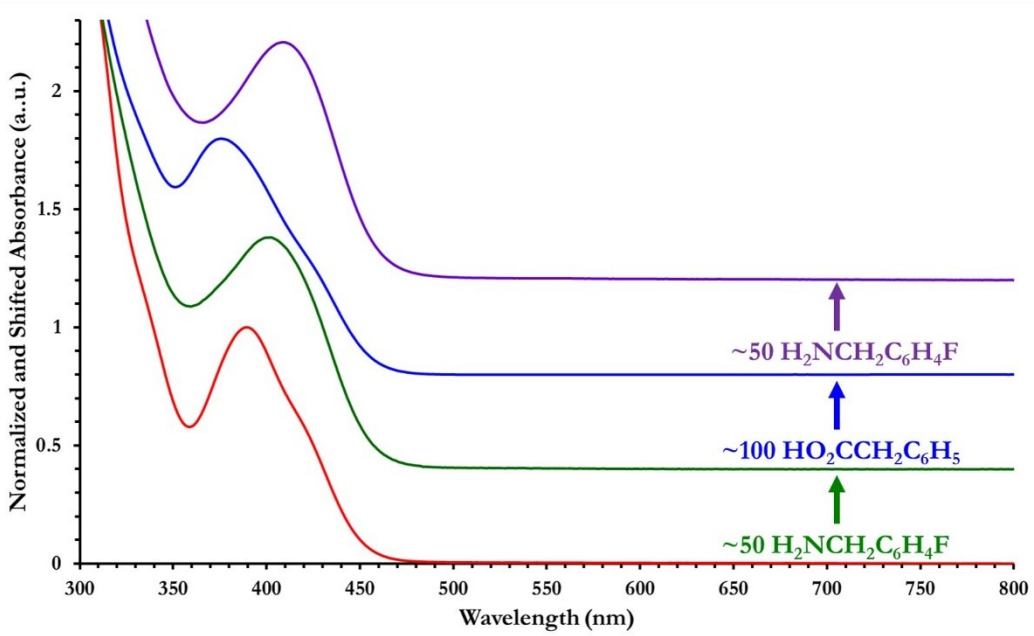

Figure S12. UV-Vis spectra of $In_{37}P_{20}(O_2CCH_2C_6H_5)_{51}$ (red spectrum) after addition of 50 equivalents of $H_2NCH_2C_6H_4F$ (green spectrum), subsequent addition of 100 equivalents of $HO_2CCH_2C_6H_5$ (blue spectrum), and finally a second addition of 50 equivalents of $H_2NCH_2C_6H_4F$ (purple spectrum). We predict that the addition of free acid is likely to remove weakly bound $H_2NCH_2C_6H_4F$ from the surface of the cluster by formation of the ammonium carboxylate salt. The shifts observed between additions of free acid and amine suggest that this effect is fully reversible.

References

1. Gary, D. C.; Cossairt, B. M. Role of Acid in Precursor Conversion During InP Quantum Dot Synthesis. *Chemistry of Materials* **25**, 2463-2469 (2013).
2. Gary, D. C.; Terban, M. W.; Billinge, S. J. L.; Cossairt, B. M. Two-Step Nucleation and Growth of InP Quantum Dots via Magic-Sized Cluster Intermediates. *Chemistry of Materials* **27**, 1432-1441 (2015).
3. M. J. Frisch *et al.* (Gaussian, Inc., Wallingford, CT, USA, 2009).
4. J. Heyd, G. E. Scuseria, M. Ernzerhof, Hybrid functionals based on a screened Coulomb potential. *The Journal of Chemical Physics* **118**, 8207-8215 (2003).
5. J. Heyd, G. E. Scuseria, Efficient hybrid density functional calculations in solids: assessment of the Heyd–Scuseria–Ernzerhof screened Coulomb hybrid functional. *The Journal of Chemical Physics* **121**, 1187-1192 (2004).
6. J. Heyd, G. E. Scuseria, M. Ernzerhof, Erratum:"Hybrid functionals based on a screened Coulomb potential"[J. Chem. Phys. 118, 8207 (2003)]. *The Journal of Chemical Physics* **124**, 219906 (2006).
7. O. A. Vydrov, J. Heyd, A. V. Krukau, G. E. Scuseria, Importance of short-range versus long-range Hartree-Fock exchange for the performance of hybrid density functionals. *The Journal of Chemical Physics* **125**, 074106 (2006).
8. E. Cho, H. Jang, J. Lee, E. Jang, Modeling on the size dependent properties of InP quantum dots: a hybrid functional study. *Nanotechnology* **24**, 215201 (2013).
9. D. C. Gary *et al.*, Single-Crystal and Electronic Structure of a 1.3 nm Indium Phosphide Nanocluster. *Journal of the American Chemical Society* **138**, 1510-1513 (2016).
10. M. E. Casida, C. Jamorski, K. C. Casida, D. R. Salahub, Molecular excitation energies to high-lying bound states from time-dependent density-functional response theory: Characterization and correction of the time-dependent local density approximation ionization threshold. *The Journal of Chemical Physics* **108**, 4439-4449 (1998).
11. F. Furche, R. Ahlrichs, Adiabatic time-dependent density functional methods for excited state properties. *The Journal of Chemical Physics* **117**, 7433-7447 (2002).
12. R. E. Stratmann, G. E. Scuseria, M. J. Frisch, An efficient implementation of time-dependent density-functional theory for the calculation of excitation energies of large molecules. *The Journal of chemical physics* **109**, 8218-8224 (1998).
13. P. Hay, T. Dunning Jr, in *Methods of Electronic Structure Theory. Schaefer III, HF (Ed.) Plenum, New York*. (1976), vol. 3, pp. 1-28.
14. P. J. Hay, W. R. Wadt, Ab initio effective core potentials for molecular calculations. Potentials for the transition metal atoms Sc to Hg. *The Journal of Chemical Physics* **82**, 270-283 (1985).
15. P. J. Hay, W. R. Wadt, Ab initio effective core potentials for molecular calculations. Potentials for K to Au including the outermost core orbitals. *The Journal of Chemical Physics* **82**, 299-310 (1985).
16. W. R. Wadt, P. J. Hay, Ab initio effective core potentials for molecular calculations. Potentials for main group elements Na to Bi. *The Journal of Chemical Physics* **82**, 284-298 (1985).